



Ru-Based Catalysts for H₂ Production from Ammonia: Effect of 1D Support

Zhigang Hu¹ · Julien Mahin¹ · Sukanya Datta¹ · Tamsin E. Bell¹ · Laura Torrente-Murciano¹

© The Author(s) 2018

Abstract

This study reveals the effect of the catalytic 1D supports (carbon, ceria, alumina and titanate) for ruthenium particles on the low temperature release of hydrogen from ammonia. While the state-of-art literature presents Ru/carbon nanotubes (CNT) as the most active catalyst, we found in this work that ruthenium supported on ceria nanorods (Ru/CeO₂) catalyst exhibited activity over 8 times higher than the Ru/CNT counterpart system. This enhanced activity is believed to be related to a strong metal-support interaction on the Ru/CeO₂ catalysts promoting the formation of small (~3 nm) Ru particles. Addition of sodium as a promoter leads to the formation of smaller Ru particle sizes in addition to the modification of the electronic environment of Ru, enhancing the ammonia decomposition activity at low temperatures. This effect is particularly noticeable in the Ru–Na/CNT catalysts, facilitated by the high conductivity of the support, allowing distant electronic modification of the Ru active sites. This work provides novel insights in designing catalysts for hydrogen production from ammonia in our effort to enable the long-term energy storage in chemical bonds.

Keywords Support effect · Ammonia decomposition · Metal–support interaction · Ruthenium catalysts · 1D nanostructures

1 Introduction

The heavy reliance of our society on fossil fuels has raised serious environmental issues mainly related to the excessive carbon dioxide (CO₂) emissions into the atmosphere [1]. One reason for this situation is the challenging and falling-behind development of new alternative renewable energy sources, such as solar, wind and biomass capable of meeting the current energy demands. Within this context, hydrogen has been presented as an attractive alternative, widely recognized as a clean energy vector to prevent further distributed pollution [2]. The implementation of the so-called *hydrogen economy* is limited by the storage and transportation of hydrogen, as well as the public perception of its safety. While newly developed porous materials (such as metal

organic frameworks) are capable of physically storing hydrogen reaching the current storage targets (~6.5 wt%), the rate of adsorption and release of H₂ as well as the required operating conditions are far from economically feasible at large scale [3]. An attractive alternative is the chemical storage of H₂ in hydrogen-rich molecules. In particular, ammonia contains 17.6 wt% hydrogen [4], it can be transported as a liquid at room temperature and mild pressure (~10 bar) and its handling regulations and shipping infrastructure for transportation already exist [5]. In spite of this, the feasibility of the *ammonia economy* depends on the development of new capabilities to release hydrogen at temperatures aligned to the operating temperature of proton exchange membrane fuel cells (PEMFCs), according to the US Department of Energy [6]. Such conditions will face thermodynamic limitations and thus, the produced hydrogen will need to be purified to avoid the poisoning of the catalyst and membrane in the fuel cells using, for example, membranes [7]. At the moment, the best reported systems for the ammonia decomposition reaction consist of ruthenium-based catalysts supported on carbon nanotubes (CNTs) [8]. Promotion of the ruthenium active species with electron donating elements enables lower temperature activity [9]. CNTs are believed to be the best catalytic support due to its promotion of Ru

Electronic supplementary material The online version of this article (<https://doi.org/10.1007/s11244-018-1058-3>) contains supplementary material, which is available to authorized users.

✉ Laura Torrente-Murciano
lt416@cam.ac.uk

¹ Department of Chemical Engineering and Biotechnology, University of Cambridge, Cambridge CB3 0AS, UK

nanoparticles with sizes between 3 and 5 nm where the B_5 active sites are maximised [10–12], as well as their high conductivity leading to $Ru^{\delta-}$ surfaces, which promotes the desorption of N-adatoms at low temperatures (the limiting step under such conditions) [4].

In order to separate both effects and to understand the role of the 1D morphology of the support on the catalyst activity, this paper investigates the ammonia decomposition activity of a range of 1D ceramic materials (ceria, titanate and alumina) as supports for Ru nanoparticles compared to the CNTs counterpart catalyst. Herein, we demonstrate that Ru supported on ceria nanorods shows the highest catalytic activity for ammonia decomposition due to its strong metal-support interaction. However the addition of an alkali metal (i.e. sodium) as a promoter does not further enhance its activity, contrary to the beneficial effect observed when Na is added to Ru-supported on 1D Al_2O_3 , titanate and CNTs supports. The largest improvement in activity upon addition of Na is observed for CNTs, likely related to their high conductivity.

2 Experimental

2.1 Synthesis of 1D Supports

Commercial multi-walled carbon nanotubes (CNTs) were purchased from NanoCyl (NC7000) and used without further treatments. Ceria rods (CeO_2 NR) were synthesized using a hydrothermal method [13]. 0.6 g of $Ce(NO_3)_3 \cdot 6H_2O$ was added to a 40 mL NaOH solution (15 M) and placed in a 45 mL PTFE lined autoclave inside an air-circulating oven at 70 °C for 10 h. The obtained powder was filtered, washed several times with deionised water and ethanol and then dried at 80 °C overnight. Alumina nanorods (Al_2O_3 NR) were synthesised using a hydrothermal method reported elsewhere [14]. 9.6 g of aluminium nitrate nonahydrate ($Al(NO_3)_3 \cdot 9H_2O$) in 40 mL deionized water was added to 20 mL of aqueous NaOH (1 M). The mixture was added to a 120 mL PTFE lined stainless steel autoclave and placed in an air-circulating oven at 200 °C for 20 h. The resulting white powder (γ -AlOOH) was separated from the solution by centrifugation (4000 rpm, 20 min), washed with deionised water, dried overnight at 80 °C under vacuum and grounded into a uniform fine powder. Finally, the γ -AlOOH powder was calcined at 500 °C for 3 h (3 °C min^{-1} heating rate) to produce γ - Al_2O_3 . Titanate nanotubes (Ti-NT) were synthesised by a hydrothermal method previously described in detail [15] using a NaOH concentration of 10 M at 130 °C for 24 h. After the synthesis, the white powder was washed with distilled water, dried under vacuum at 80 °C, washed with a 0.1 M H_2SO_4 solution until the supernatant reached

a pH of 7 and finally the powder was washed with deionised water.

2.2 Synthesis of Catalysts

Ruthenium was supported on the different 1D supports by incipient wetness impregnation of ruthenium nitrosyl nitrate aqueous solutions. The wetness impregnation volumes for Al_2O_3 NR, CNT, Ti-NT and CeO_2 NR were measured as 1.2, 10, 1, 1.2 mL g^{-1} respectively using water as a solvent. After impregnation of aqueous solutions, the catalysts were dried at 80 °C under vacuum for 24 h.

2.3 Characterization Methods

Powder X-ray diffraction (PXRD) patterns were obtained on a Bruker D8 Advance X-ray powder diffractometer equipped with a Cu sealed tube ($\lambda = 1.54178 \text{ \AA}$) at a scan rate of 0.02° s^{-1} . High-resolution transmission electron microscopy (HR-TEM) images were recorded on a FEI Tecnai F20 operated at 200 kV. Nitrogen sorption isotherms were measured up to 1 bar using a Micromeritics ASAP 2020 surface area and pore size analyzer. Before the measurements, the samples were degassed under reduced pressure ($< 10^{-2}$ Pa) at 120 °C for 6 h. Ultra high purity (UHP) grade N_2 is used for all the measurements. Temperature programme reduction (TPR) and CO pulse chemisorption were carried out using a Micromeritics AutoChem II with a thermal conductivity detector. TPR analyses were performed with 30 mL min^{-1} of 5% H_2/Ar with a ramp rate of 10 °C min^{-1} . CO chemisorption of the catalysts was carried out at 35 °C using 5% CO/He to estimate the metallic surface area and calculate the average particle size [16] using a stoichiometric factor for CO:Ru of 1:1.

2.4 Ammonia Decomposition Tests

Ammonia decomposition activity of the different catalysts was evaluated in a catalytic bespoke flow rig using 25 mg of catalyst diluted in 4 mL silicon carbide bed (450 mg) inside a quartz U-shaped reactor. Prior to testing, the catalysts were pre-reduced in situ at 300 °C for 30 min using 10 N mL min^{-1} of pure H_2 . The furnace temperature was controlled by an external furnace (Carbolite) with a type K thermocouple located directly above the catalyst bed. All the gas supply tubing was heated to 60 °C to avoid any ammonia condensation and consequent corrosion. A mixture of NH_3 and He (1:2.4 molar ratio) was flowed continuously through the reactor with a gas hourly space velocity (GHSV) of 6000 mL $_{NH_3}$ g_{cat}^{-1} h^{-1} . During the catalytic test, the furnace temperature was ramped from ambient temperature to 550 °C at a rate of 2.6 °C min^{-1} for three consecutive cycles where the temperature is increased and decreased. The

composition of the outlet gas stream was analysed online using a gas chromatographer with a Propak Q column and a thermal conductivity detector. The mass balance was closed with $\pm 10\%$ error. The activation energy was calculated at low levels of conversion ($< 20\%$) to assume a constant apparent rate of reaction.

3 Results and Discussion

To fully understand the effect of the 1D morphology of the support of the Ru-based catalysts on the ammonia decomposition activity, 1D materials including carbon nanotubes (CNT), ceria nanorods (CeO_2 NR), alumina nanorods (Al_2O_3 NR) and titania nanotubes (Ti-NT) were used as catalytic supports. Figure 1 shows representative TEM pictures of the different pristine supports showing the high aspect ratio of the different materials. Commercial CNTs and Ti-NTs have a hollow structure while CeO_2 NR and Al_2O_3 NR have a solid interior. In terms of dimensions, the four materials show different length distributions with average values of 1 μm , 200 nm, 50 nm and 100 nm for CNT, Ti-NT, CeO_2

NR and Al_2O_3 NR respectively. In all cases, the 1D materials have diameters within the same scale of 10–20 nm.

Ruthenium nanoparticles were loaded on the different 1D supports by incipient wetness impregnation followed by in situ reduction at 300 $^\circ\text{C}$ under H_2 flow. Figure 2 shows the catalytic activity for the ammonia decomposition reaction of the 7 wt% Ru catalysts as a function of temperature. The Ru/ CeO_2 catalyst shows the highest reaction rate, with an onset activity temperature as low as ~ 270 $^\circ\text{C}$, considerably lower than when Ru is supported on the other 1D supports (~ 350 $^\circ\text{C}$), including CNTs. The trend of catalytic activity follows the order of CeO_2 NR \gg Ti-NT $>$ Al_2O_3 NR $>$ CNT. The same trend is observed for the activation energy values, decreasing from 110 kJ mol^{-1} for the Ru/ Al_2O_3 catalysts to 82.5 kJ mol^{-1} for Ru/ CeO_2 , which indicates a clear effect of the support material on the resulting Ru active sites. Note that the catalyst supported in Ti-NT contains a substantial amount of sodium as discussed below.

Powder X-ray diffraction (PXRD) confirms the crystallinity of the different 1D ceramic supports (Fig. 1S), corresponding to the γ -phase of alumina [17], titanate [18] and face centred cubic phase of CeO_2 nanorods respectively [19]. After the loading of the Ru nanoparticles and H_2 reduction

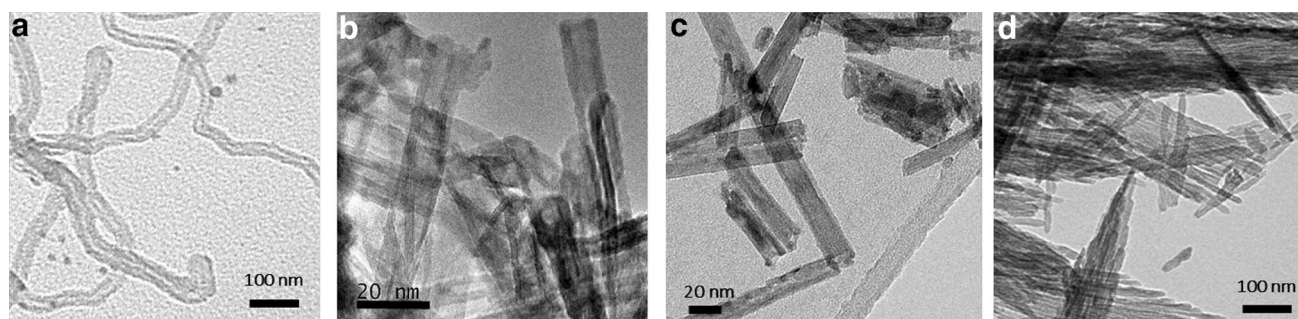


Fig. 1 High aspect ratio materials used as catalytic support for Ru NPs: **a** commercial CNTs; **b** titanate nanotubes; **c** ceria nanorods; and **d** alumina nanorods

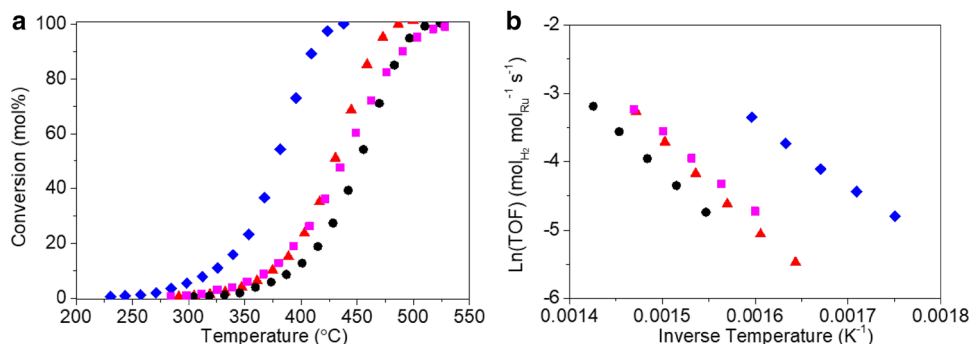


Fig. 2 Catalytic activity of 7 wt% Ru catalysts supported on 1D supports: **a** ammonia decomposition conversion as a function of temperature; **b** Arrhenius plot. Filled triangle Ru/ Al_2O_3 NR, filled circle Ru/

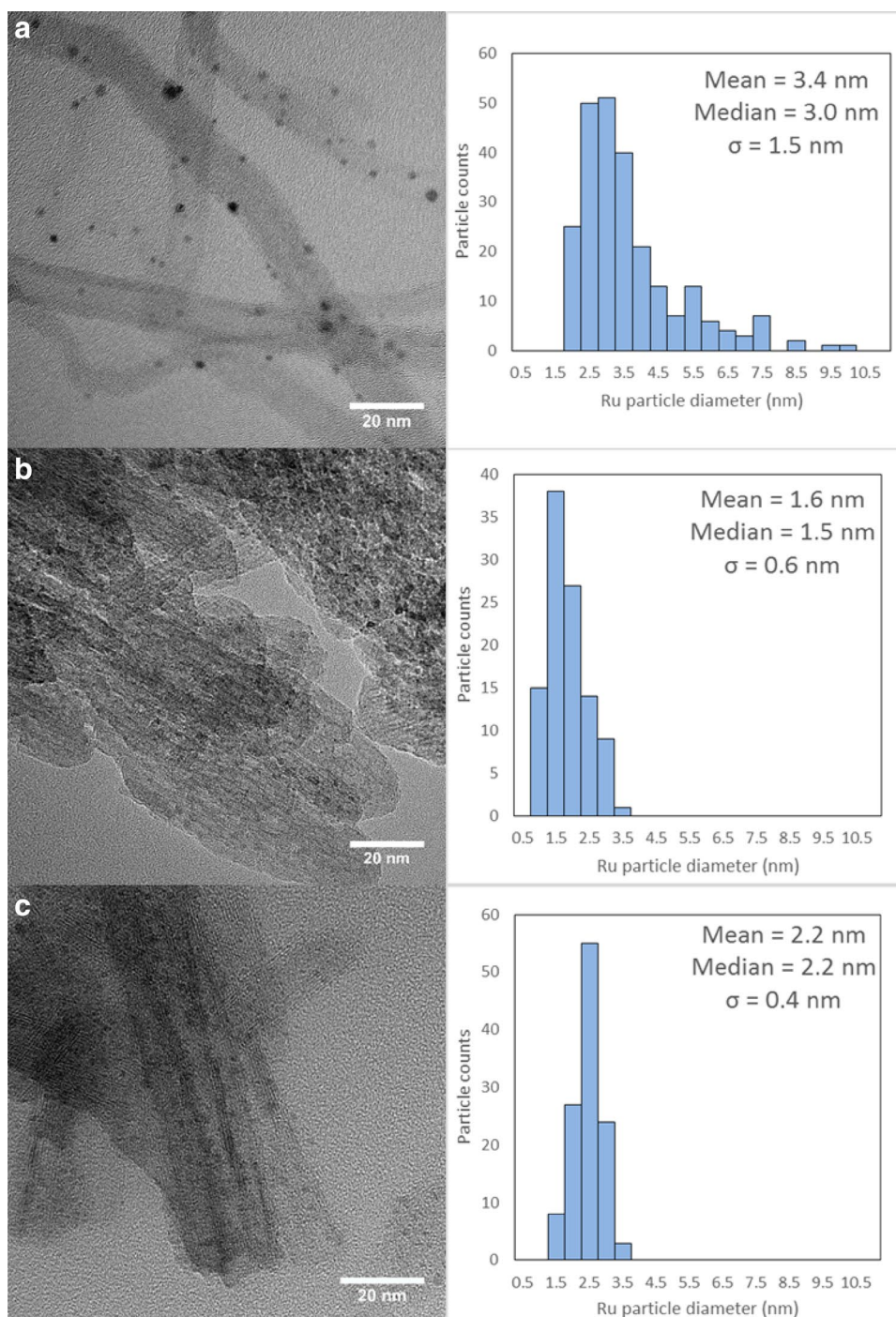
CNT, filled square Ru-Na/Ti-NT, filled diamond Ru/ CeO_2 NR. Reaction conditions: 2.5 mL min^{-1} NH_3 , 6 mL min^{-1} He, 25 mg catalyst, GHSV: 6000 h^{-1} . Catalysts are pre-reduced at 300 $^\circ\text{C}$ under H_2 flow

at 300 °C, there are no obvious diffraction peaks at 38° and 44° assigned to the (100) and (002) crystal planes of the hexagonal close-packed (hcp) Ru metal nanoparticles [20–22] in any of the catalysts. In the case of the Ru/Al₂O₃ NR and Ru/CeO₂ NR catalysts, a diffraction peak at 24° associated to the hexagonal close-packed (hcp) (210) Ru plane is observed [20–22]. Due to the low signal-to-noise ratio, it is not possible to accurately estimate the particle size by the Scherrer equation [23], however, these observations suggest that the

Ru average particle size is below 3 nm, based on the detection limit of XRD [24].

Figure 3 shows representative TEM images of the 7 wt% Ru catalysts as well as the ruthenium particle size histogram. Ru particle size lies within the range 1.5–3.5 nm, with Ru/CNT showing the biggest (3.4 ± 1.5 nm) and Ru/Al₂O₃ NR the smallest (1.6 ± 0.6 nm) average ruthenium particle sizes. Due to the low contrast between Ru and Ce arising from their similar atomic numbers, it was

Fig. 3 TEM micrographs and Ru particle size distributions for 7 wt% Ru catalysts: **a** Ru/CNT; **b** Ru/Al₂O₃ NR; **c** Ru–Na/Ti–NT. Catalysts were pre-reduced at 300 °C under H₂ flow



not possible to image the metal particles in the Ru/CeO₂ NR catalyst suggesting particle sizes < 2 nm (Fig. S2). CO chemisorption at 35 °C after in situ H₂ reduction at 300 °C was also performed to evaluate the Ru particle size, assuming a CO:Ru stoichiometric factor of 1:1 [16]. The calculated Ru NP sizes for Ru/Al₂O₃ NR, Ru/CNT, Ru/Ti-NT and Ru/CeO₂ NR catalysts are 4.3, 5.8, 7.6 and 3.2 nm respectively (Table 1). The Ru particle sizes estimated using CO chemisorption are considerably bigger than those observed by microscopy. This discrepancy is likely to be associated to the assumption of hemispherical shape made in the calculations based on CO chemisorption [16], suggesting the 1D morphology of the supports promotes the flattening of the nanoparticles as we have

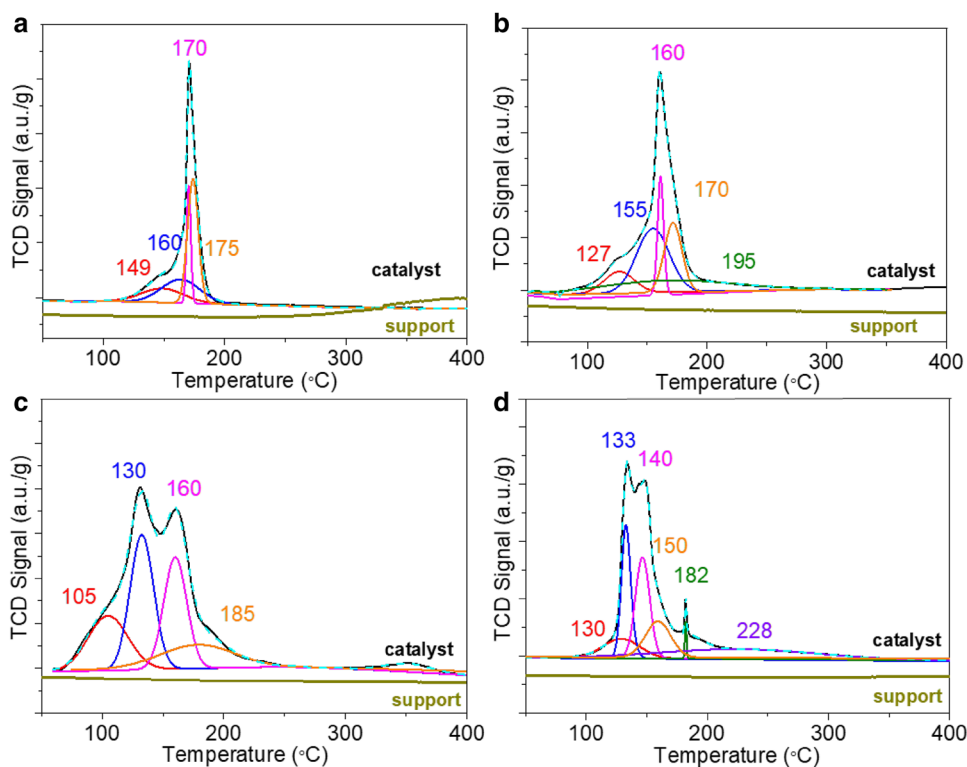
previously observed for Ti-NT supported catalysts [25, 26].

Temperature programmed reduction (TPR) profiles of the different 7 wt% Ru catalysts are shown in Fig. 4. TPR curves are deconvoluted with no weighting method. In all cases, the pristine supports do not show any comparable reduction within the studied range of temperature. Ru particles in Ru/CeO₂ NR and Ru/Ti-NT catalysts are reduced at the lowest temperatures, despite presenting different Ru sizes (3.2 and 7.6 nm respectively based on CO chemisorption). Considering the small size of the Ru nanoparticles in the Ru/CeO₂ catalyst, one would expect a shift towards high reduction temperatures however, the low reduction temperature (130–150 °C) suggests that the CeO₂ NR support

Table 1 Physical and catalytic properties of 7 wt% Ru catalysts supported on 1D materials

Catalyst	Surface area m ² g ⁻¹	Ru NP size (nm)		Na content by ICP (wt%)	Metallic surface area (m ² g _{Ru} ⁻¹)	Activa- tion energy (kJ mol ⁻¹)	TOF @ 350 °C (mol _{H₂} mol _{Ru} ⁻¹ h ⁻¹)
		TEM	CO chem- isorption				
7 wt% Ru/CNT	220	3.4 ± 1.5	5.8	0.7	83.9	103.8	13.0
7 wt% Ru 7 wt% Na/CNT	200	1.9 ± 0.5	2.8	7	175.8	84.7	316.7
7 wt% Ru/Al ₂ O ₃ NR	50	1.6 ± 0.6	4.3	1.6	115.2	110.8	22.9
7 wt% Ru 7 wt% Na/Al ₂ O ₃ NR	35	2.1 ± 0.4	4.1	7	119.8	95.4	112.3
7 wt% Ru 7 wt% Na/Ti-NT	70	2.2 ± 0.5	7.6	7.1	61.6	95.6	32.1
7 wt% Ru/CeO ₂ NR	15	–	3.2	0.2	150.5	82.5	122.4
7 wt% Ru 7 wt% Na/CeO ₂ NR	10	–	2.9	7	165.6	85.9	165.6

Fig. 4 Temperature programmed reduction profile for pristine and 7 wt% Ru catalysts loaded 1D supports: **a** Ru/Al₂O₃ NR; **b** Ru/CNT; **c** Ru–Na/Ti-NT; **d** Ru/CeO₂ NR



plays a role in the reducibility of the Ru active sites, [27, 28]. Indeed, recent studies have recently demonstrated that oxygen vacancies on the ceria surface can strongly bind to the Ru NPs, explaining its high catalytic activity, especially at low temperatures in comparison to the other 1D supports.

As the 1D oxide supports herein are synthesised using alkali-based hydrothermal methods, inductively coupled plasma atomic emission spectroscopy (ICP-AES) was used to determine the content of Na in the catalysts. Alkali metals, such as sodium, are known to have a promotion effect on the catalytic activity of Ru nanoparticles for the ammonia decomposition reaction [9, 29]. Ru/Ti-NT contains 7.1 wt% Na, which is considerably higher than that of the other three catalysts which contain ~0.2–0.7 wt% (Table 1). To understand the effect of the presence of sodium on the activity, a series of catalysts were prepared with 7 wt% Ru and 7 wt% Na by consecutive impregnation of the supports by sodium followed by ruthenium. Figure 5 shows the ammonia decomposition catalytic activity of the different Ru–Na catalysts. The trend in catalytic activity of the catalysts varies considerably with the presence of Na as CNT > CeO₂ NR ~ Al₂O₃ NR > Ti-NT. It is important to note that the presence of Na enhances the catalytic activity of the catalysts to different extent as a function of the support used. While the apparent rate of reaction at 350 °C of the Ru–Na/CNT catalysts increases by 24 times from 13.0 to 316.7 mol_{H₂} mol_{Ru}⁻¹ h⁻¹ by addition of Na, only a fourfold increase is observed for the Ru–Na/Al₂O₃ NR catalyst from 22.9 to 112.3 mol_{H₂} mol_{Ru}⁻¹ h⁻¹. Interestingly, almost no effect of the addition of sodium is observed in the case of Ru–Na/CeO₂ NR. Even more important than the increase in activity generally observed by the addition of sodium is the downward shift of the onset activity temperature towards lower temperatures. Again, the major effect is observed in the case of the Ru–Na/CNT catalysts with the onset activity temperature shifting from ~350 to ~250 °C by addition of

sodium. A smaller effect is observed in the catalysts using ceramic 1D supports.

TEM micrographs of the Ru–Na catalysts are shown in Fig. 6. As mentioned before, it was not possible to image the Ru particles when supported on CeO₂ NR, while the Ru–Na/Ti-NT images are shown in Fig. 3. A similar dispersion of the Ru particles is observed when compared to the images in the absence of sodium (Fig. 3). However, an important decrease in particle size is observed in the Ru–Na/CNT catalyst (1.9 nm) in comparison to the Ru/CNT counterpart (3.4 nm). This trend of reduced particle size in the presence of sodium is further confirmed by CO chemisorption, with sizes of 4.1, 2.8, 7.6 and 2.9 nm for the Ru–Na/Al₂O₃ NR, Ru–Na/CNT, Ru–Na/TiO₂ NT, Ru–Na/CeO₂ NR, respectively (Table 1). One should note that sodium was first impregnated in the support, followed by ruthenium and thus, it is unlikely that sodium is partially covering the surface of the active sites as previously observed when the impregnation of the promoters is post-synthesis of the catalysts [8].

Indeed, there seems to be a relationship between the Ru particle size and the ammonia decomposition catalytic activity of both the Ru and the Ru–Na catalysts as shown in Fig. 7, with an exponential increase in catalytic activity observed as the Ru size decreases. This effect seems to be independent of the presence of sodium although related to the decrease in particle size. It is possible that the enhanced activity of the Ru–Na/CNT catalyst is achieved by a combination of the smaller Ru particle size and the high conductivity of the CNT support, which enables electronic modification of the Ru active sites [9].

TPR experiments provide further insights into the role of sodium as promoter. Figure 8 shows a shift towards higher reduction temperatures for the Ru–Na/CNT and Ru–Na/Al₂O₃ NR catalysts in comparison to their Ru-only counterparts (Fig. 4) in agreement with their smaller Ru sizes and a stronger metal-support interaction, responsible for their enhanced

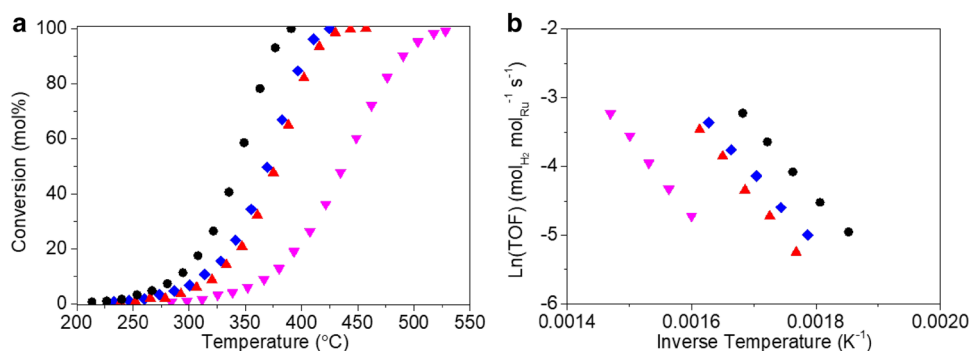


Fig. 5 Catalytic activity of 7 wt% Ru–7 wt% Na catalysts supported on 1D supports: **a** ammonia decomposition conversion as a function of temperature; **b** Arrhenius plot. Filled triangle Ru–Na/Al₂O₃ NR, filled circle Ru–Na/CNT, filled inverted triangle Ru–Na/Ti-NT, filled

diamond Ru–Na/CeO₂ NR. Reaction conditions: 2.5 mL min⁻¹ NH₃, 6 mL min⁻¹ He, 25 mg catalyst, GHSV: 6000 h⁻¹. Catalysts are pre-reduced at 300 °C under H₂ flow

Fig. 6 TEM micrographs and Ru particle diameter distributions for reduced catalysts: **a** Ru–Na/CNT; **b** Ru–Na/Al₂O₃ NR. Catalysts are pre-reduced at 300 °C under H₂ flow

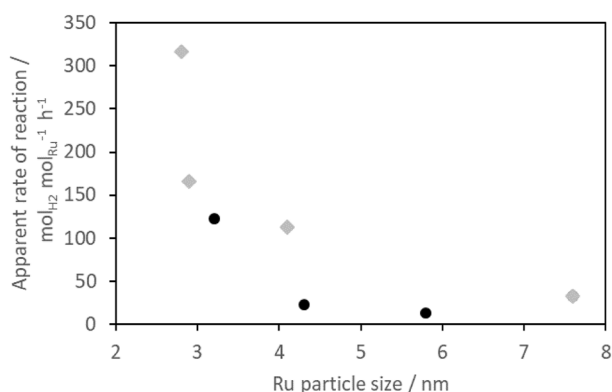
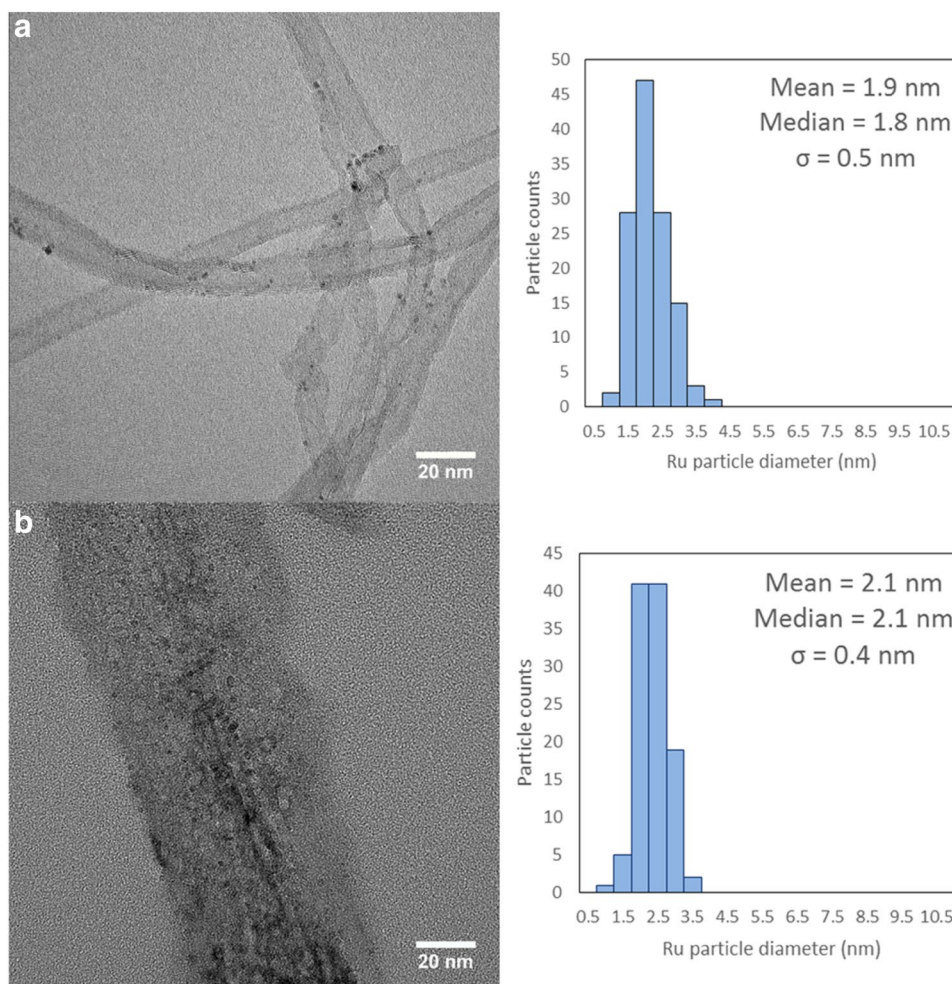


Fig. 7 Relationship between Ru particle size (from CO chemisorption) and apparent ammonia decomposition rate of reaction at 350 °C. Filled circle 7 wt% Ru catalysts, filled diamond 7 wt% Ru–7 wt% Na catalysts

ammonia decomposition activity. Interestingly, a similar TPR profile is observed in both the Ru- and the Ru–Na/CeO₂ NR catalysts in agreement with their similar catalytic activities.

Finally, the stability of the different catalysts was evaluated by thermal cycles during the catalytic tests (Fig. 9). There is no noticeable decrease in activity after each consecutive run for Ru–Na/Al₂O₃ NR, Ru–Na/CNT and Ru–Na/CeO₂ NR catalysts, indicating their excellent stability versus sintering of the Ru nanoparticles. This is in agreement with the flattening of the metal particles mentioned above when using 1D supports. However, there is a decrease in activity after each consecutive run for Ru–Na/Ti-NT catalyst, suggesting sintering of the Ru particles under reaction conditions.

4 Conclusions

A range of high aspect ratio materials including carbon nanotubes, titanate nanotubes, ceria rods and alumina rods have been investigated as supports for ruthenium

Fig. 8 Temperature programmed reduction profile for 7 wt% Ru–7 wt% Na catalysts supported on 1D supports: **a** Al₂O₃ NR; **b** CNT; **c** Ti-NT; **d** CeO₂ NR

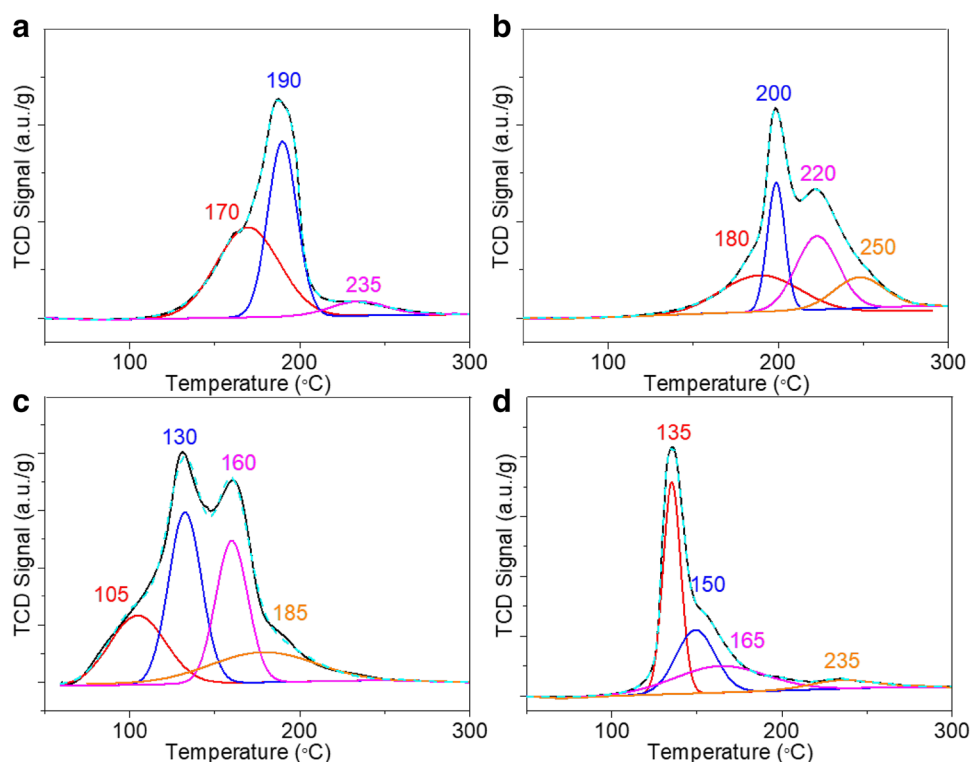
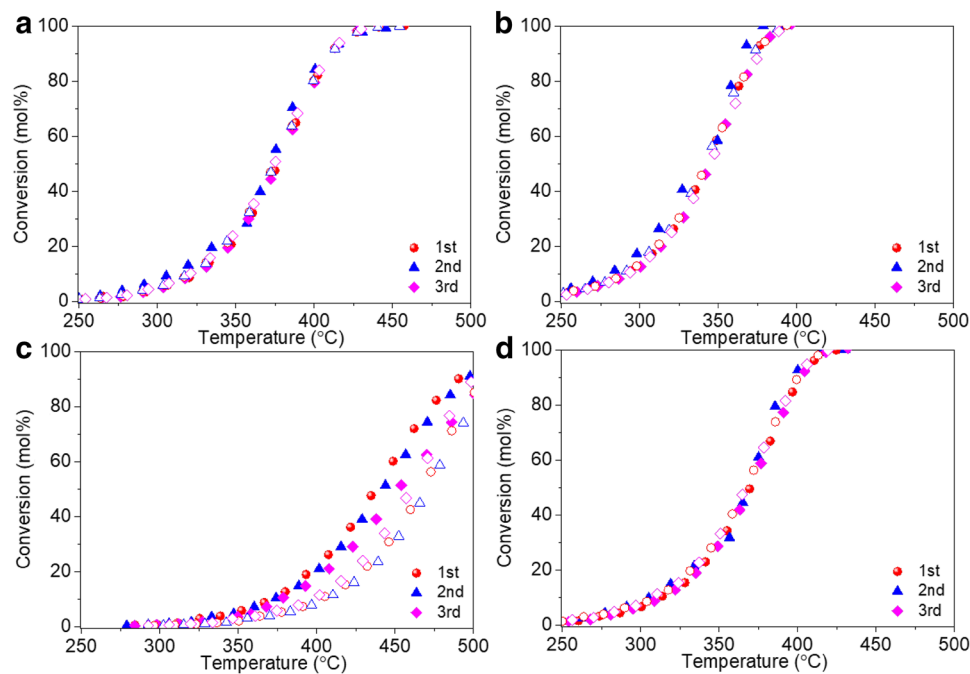


Fig. 9 Cyclic ammonia decomposition stability tests of the 7 wt% Ru–7 wt% Na catalysts: **a** Ru–Na/Al₂O₃ NR; **b** Ru–Na/CNT; **c** Ru–Na/Ti-NT; **d** Ru–Na/CeO₂ NR



nanoparticles to elucidate the effect of the 1D morphology of the support on the resulting catalytic activity for hydrogen production from ammonia. In all cases, the high aspect ratio of the supports seems to promote the flattening of the Ru nanoparticles. In the absence of promoters, the Ru/CeO₂ rods catalyst shows the highest activity at low temperatures

(270 °C), which is believed to be related to the strong metal-support interaction and the electronic modification of the Ru active sites by the ceria support. Addition of sodium to the catalyst as an electron donating promoter enhances the activity of the Ru–Na catalysts associated to the promotion of smaller Ru particles and their electronic modification,

facilitating desorption of N-atoms from the catalyst surface at lower temperatures. While this promotion effect of sodium is particularly enhanced when using CNTs as support due to their high conductivity, it has a negligible effect on the CeO₂-based catalysts.

Acknowledgements The authors would like to acknowledge the UK Engineering and Physical Science Research Council (Grant Number EP/N013778/1) for funding. LTM is thankful for the Fellowship Award (EP/L020432/2).

Open Access This article is distributed under the terms of the Creative Commons Attribution 4.0 International License (<http://creativecommons.org/licenses/by/4.0/>), which permits unrestricted use, distribution, and reproduction in any medium, provided you give appropriate credit to the original author(s) and the source, provide a link to the Creative Commons license, and indicate if changes were made.

References

- INTERNATIONAL ENERGY OUTLOOK (2016) <https://www.eia.gov/forecasts/ieo/world.cfm>. Accessed May 2018
- Ball M, Wietschel M (2009) The hydrogen economy: opportunities and challenges. Cambridge University Press, New York
- Zhang C (2016) Hydrogen storage: letting it go. *Nat Energy* 1:15022
- Bell TE, Torrente-Murciano L (2016) H₂ production via ammonia decomposition using non-noble metal catalysts: a review. *Top Catal* 59(15):1438–1457
- Giddey S et al (2017) Ammonia as a renewable energy transportation media. *ACS Sustain Chem Eng* 5(11):10231–10239
- Bakangura E et al (2016) Mixed matrix proton exchange membranes for fuel cells: state of the art and perspectives. *Prog Polym Sci* 57:103–152
- Garcia-Garcia FR et al (2012) Hollow fibre membrane reactors for high H₂ yields in the WGS reaction. *J Membr Sci* 405:30–37
- Hill AK, Torrente-Murciano L (2014) In-situ H₂ production via low temperature decomposition of ammonia: insights into the role of cesium as a promoter. *Int J Hydrog Energy* 39(15):7646–7654
- Hill AK, Torrente-Murciano L (2015) Low temperature H₂ production from ammonia using ruthenium-based catalysts: synergistic effect of promoter and support. *Appl Catal B* 172–173:129–135
- Garcia-Garcia FR, Guerrero-Ruiz A, Rodriguez-Ramos I (2009) Role of B5-type sites in Ru catalysts used for the NH₃ decomposition reaction. *Top Catal* 52(6–7):758–764
- Torrente-Murciano L, Hill AK, Bell TE (2017) Ammonia decomposition over cobalt/carbon catalysts-effect of carbon support and electron donating promoter on activity. *Catal Today* 286:131–140
- Garcia-Garcia FR et al (2010) The use of carbon nanotubes with and without nitrogen doping as support for ruthenium catalysts in the ammonia decomposition reaction. *Carbon* 48(1):267–276
- Torrente-Murciano L et al (2013) Shape-dependency activity of nanostructured CeO₂ in the total oxidation of polycyclic aromatic hydrocarbons. *Appl Catal B* 132–133:116–122
- Bell TE et al (2015) Single-step synthesis of nanostructured γ -alumina with solvent reusability to maximise yield and morphological purity. *J Mater Chem A* 3(11):6196–6201
- Torrente-Murciano L, Lapkin AA, Chadwick D (2010) Synthesis of high aspect ratio titanate nanotubes. *J Mater Chem* 20(31):6484–6489
- Torrente-Murciano L (2016) The importance of particle-support interaction on particle size determination by gas chemisorption. *J Nanopart Res* 18:87
- Bell TE et al (2018) High yield manufacturing of γ -Al₂O₃ Nanorods. *ACS Sustain Chem Eng* 6(1):88–92
- Walsh FC et al (2006) Synthesis of novel composite materials via the deposition of precious metals onto protonated titanate (TiO₂) nanotubes. *Trans Inst Metal Finish* 84(6):293–299
- Hammond OS et al (2017) Deep eutectic-solvothermal synthesis of nanostructured ceria. *Nat Commun* 8:14150
- Liu J, Bai P, Zhao XS (2011) Ruthenium nanoparticles embedded in mesoporous carbon microfibers: preparation, characterization and catalytic properties in the hydrogenation of d-glucose. *Phys Chem Chem Phys* 13(9):3758–3763
- Zhang Q et al (2018) Selective control of fcc and hcp crystal structures in Au–Ru solid-solution alloy nanoparticles. *Nat Commun* 9(1):510
- Pan X et al (2014) Towards a highly dispersed and more thermally stable Ru/OCNT catalyst. *Chem Commun* 50(29):3856–3858
- Patterson AL (1939) The Scherrer formula for X-ray particle size determination. *Phys Rev* 56(10):978–982
- Hargreaves JSJ (2016) Some considerations related to the use of the Scherrer equation in powder X-ray diffraction as applied to heterogeneous catalysts. *Catal Struct React* 2(1–4):33–37
- Torrente-Murciano L, Villager T, Chadwick D (2015) Selective oxidation of salicylic alcohol to aldehyde with O₂/H₂ using Au–Pd on titanate nanotubes catalysts. *ChemCatChem* 7(6):925–927
- Torrente-Murciano L et al (2014) Enhanced Au–Pd activity in the direct synthesis of hydrogen peroxide using nanostructured titanate nanotube supports. *ChemCatChem* 6(9):2531–2534
- Torrente-Murciano L et al (2016) Effect of nanostructured ceria as support for the iron catalysed hydrogenation of CO₂ into hydrocarbons. *Phys Chem Chem Phys* 18(23):15496–15500
- Mamontov E et al (2000) Lattice defects and oxygen storage capacity of nanocrystalline ceria and ceria-zirconia. *J Phys Chem B* 104(47):11110–11116
- Mukherjee S et al (2018) Low-temperature ammonia decomposition catalysts for hydrogen generation. *Appl Catal B* 226:162–181